Chapter 2

Slowing antiprotons

Antiprotons are produced and then decelerated to 5.9 MeV energy at CERN. Slowing of antiprotons from LEAR energies of 5.9 or 21 MeV, down to keV energies is accomplished by sending the beam through a degrader which consists mainly of thin foils of mylar, Ti, Be, and Al. Various gases provide fine adjustment of thickness of the degrader. We prepared a simple time-of-flight spectrometer to study the range curve and the transmitted particle energy distribution. Particular interest is in the low energy particle yield since those particles can be trapped in an ion trap for further studies.

2.1 Production and deceleration of antiprotons at CERN

Antiprotons are generated at CERN by impinging 26 GeV protons on a heavy target [34,35]. Fig. 2.1 shows the facility for antiproton production at CERN. First, protons are obtained in the Pre-injector where electrons are stripped off from hydrogen atoms by ionization. Protons then are accelerated to 50 MeV in a linear accelerator (LINAC). In the next stage, the Booster increases the proton energy to 1 GeV. At the Proton Synchrotron (PS) ring proton energy reaches 26 GeV. A

high-intensity 26 GeV proton beam is sent to the antiproton production area and directed onto the target. Negative secondaries in a 6% momentum bite around 3.5 GeV/c (2.7 GeV) are selected and transferred to the Antiproton Collector (ACOL) ring. After bunch rotation and stochastic cooling, the antiproton beam is transferred into the Antiproton Accumulator (AA) and then stochastically cooled. In the stochastic cooling process, the longitudinal and transverse random motions of the antiproton beam are first detected. Then the signals are fed back to suppress the antiprotons momentum spread and transverse emittances. Typically a momentum spread $\Delta p/p$ of a few parts in 10^3 can be achieved by stochastic cooling [36].

The 26 GeV proton beam consists of five proton bunches, each containing 2×10^{12} protons. Every beam of five bunches hits the target in a burst of $0.5\mu s$ duration. This can be repeated every 2.4 s or in multiples of this period, mostly 4.8 sec. The bunch length in every beam is 20 ns and the time between bunches is 110 ns. The beam is focused at the target with small divergence of 2 mrad, and 95% of the beam hits a circular spot of 1 mm radius which is smaller than the target wire radius of 1.5 mm. The metal target being used at present is a 55 mm long iridium wire, which is along the direction of the beam, because of its high antiproton yield and high thermal conductivity for cooling. Other metals such as copper and tungsten were used before. The iridium wire is pressed into a graphite cylinder and sealed in a titanium alloy container cooled by water. The iridium wire and a 20 mm diameter lithium magnetic lens are in a very compact assembly. The lithium lens is used to focus antiprotons when a current pulse synchronized with the antiproton beam bunch flows through a cylinder of solid lithium. A magnetic field is created and the Lorentz force steers antiprotons back toward the beam axis.

The present antiproton production yield is 5×10^{-6} $\overline{p}/p$. This corresponds to a maximum production rate of 7.5×10^{10} $\overline{p}$/hr for a beam of 10^{13} protons every

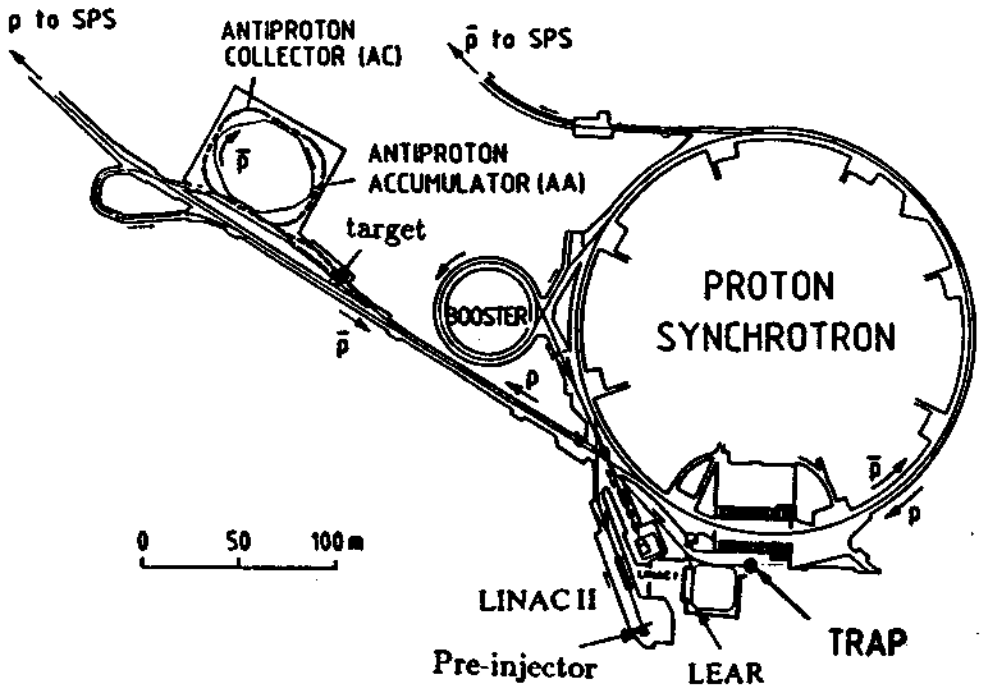

Figure 2.1: CERN facility for producing, transferring, storing and cooling antiprotons.

2.4 sec. Accumulation rates are about 30% to 50% of the production rates due to losses during the collection and stacking processes. Therefore the overall production and accumulation efficiency for 3.5 GeV/c antiprotons is about 2×10^{-6} $\overline{p}/p$ which is 3×10^{10} $\overline{p}$/hr.

Cooled antiprotons from the AA are decelerated in the PS from momentum of 3.5 GeV/c to 609 MeV/c (180 MeV). The decelerated antiprotons are transferred to the LEAR, the unique facility for providing large numbers of low energy antiprotons suitable for the trapping experiments. It is a square with side length of 20 meters. Typically 3×10^9 particles are transferred from the PS in each fill which takes up to 10 minutes including setup time. They are decelerated from 609 MeV/c to 309 MeV/c, then to 200 MeV/c, and finally to 105 MeV/c (5.9 MeV) within 20 minutes. The beam lifetime at 5.9 MeV is approximately one hour. Stochastic cooling is used again in the LEAR machine to reduce the energy spread and transverse emittances before and after each deceleration. The momentum spread $\Delta p/p$ is typically 10^{-3}. The well tuned beams of low energy antiprotons with energy as low as 5.9 MeV are extracted to the experimental area. The LEAR machine provides beams in two ways. Slow extraction is the normal mode of operation in which a slow and uniform spill of up to 10^9 particles is sent to experiments over approximately 1 h with rates from 10^3 to 10^5 Hz. Fast extraction is a special operation mode developed for the antiproton trapping experiment in which a 300 ns pulse containing up to 3×10^8 antiprotons is sent to our TRAP experiment.

The zone layout of our TRAP experiment (PS196) is shown in Fig. 2.2. The beam from LEAR in a horizontal beam line with a height of 1.6 m is bent by two dipole magnets (each one bending the beam 45^0 with a 0.3 Tesla field) into the vertical direction. A quadrupole focusing magnet is located between the two bending magnets. The last dipole magnet (Fig. 2.2) has a height of 3.1 m. The distance between its center and the center of our magnet is 1.7 m. The configuration of

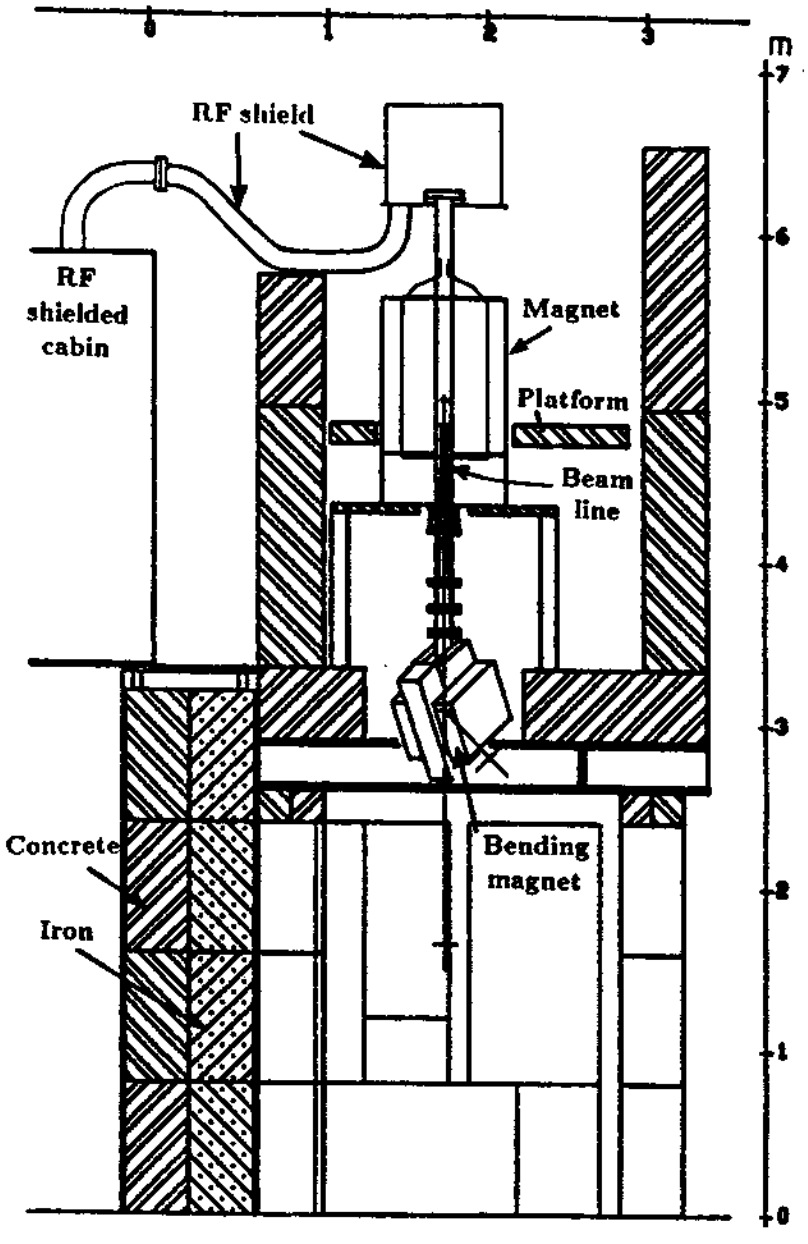

Figure 2.2: The zone layout of the TRAP experiment (PS196).

two 45^0 bending magnets allows focusing particles which differ slightly in energy to the same entrance to our apparatus. This feature is not possible for a single 90^0 magnet. Our extension of the LEAR beamline protrudes up into the bore of the superconducting solenoid and has an extremely thin Ti window just below the solenoid center (to minimize the multiple scattering effects, see Chapter 3). The Ti window separates the LEAR vacuum and 1 atm environment. Electronics for antiproton trapping studies are in a radio frequency (RF) shielded cabin, since there are strong RF noise sources in the experimental hall. There is an aluminum cap on the top of the magnet for RF shielding. Cables between the trap apparatus and the RF cabin (mostly double shielded cables) are within a flexible aluminum tube preventing external RF interference from leaking into our system.

2.2 The stopping and range of ions in matter

Energetic heavy charged particles (particle mass is much larger than electron mass m) in matter interact with atomic electrons and nuclei. The collisions with atomic electrons in matter constitute the main cause of energy loss by excitation and ionization of atoms or molecules, while nuclear scattering determines the spatial distribution of particle trajectories.

The average energy loss per unit path length is called the stopping power, S = −dE/dx, where E is the particle kinetic energy, and x is the absorber thickness. The stopping power [37] is the summation (and integration for ionized states) of each collision cross section σ_n times the corresponding energy transition E_n:

$$S = N\Sigma_n E_n \sigma_n \tag{2.1}$$

where N is the density of atoms in the target. For a heavy particle of charge Z and velocity v passing through a medium of atomic number Z_t, the stopping power S

is given as [38]:

$$S = -dE/dx = (4\pi e^4/mv^2)NZ_tZ^2L \tag{2.2}$$

where m is the electron rest mass, NZ_t is the electron density n_e in the matter, and L is a function of the particle velocity and stopping material. Using the Bethe stopping function, we have [38]

$$L = L_0(v, Z_t) = \ln(2mv^2/I) - \ln(1 - v^2/c^2) - v^2/c^2 - C/Z_t. \tag{2.3}$$

Here, I is the target mean-excitation and ionization potential (it is 166 eV for Al), and C/Z_t is the shell correction. The stopping power for heavy charged particles depends largely on the velocity and the charge of the particle, but not on its mass. For proton energies above 100 keV the smaller the velocity, the larger dE/dx is. Therefore more energy loss per unit length will happen near the final stage of slowing.

A theoretical range is obtained by integrating the inverse stopping power over the total energy loss [37]. A parallel monoenergetic beam of heavy charged particles in matter has a relatively well defined range, which is essentially the thickness of the absorber stopping practically all the particles. (The energy loss is not like the exponential absorption for the electromagnetic radiation.) In Fig. 2.3(a), a range curve shows the fraction of particles in a beam penetrating to a given depth x. Initially the beam loses energy in matter without changing the number of the particles in the beam. All the particles go a long way together. When the thickness of the absorber is very close to the range, the number of particles starts to decrease rapidly. The mean range R_0 is the thickness of the absorber allowing 50% of the particles to pass. Particles do not stop sharply at R_0 because of the statistical nature of the energy loss process. Random interactions produce fluctuations in energy loss or in range. Straggling is just the fluctuation in energy loss or the particle penetration depth (range). For a given energy loss, each particle stops near the average value R_0 with its own range R. For particles with a mean value

R_0, the probability of finding a particle with range between R and R+dR is [37]:

$$f(R)dR \approx (1/\sigma\sqrt{2\pi})exp[-(R-R_0)^2/2\sigma^2]dR. \quad (2.4)$$

Here, the distribution function f(R) of ranges around the average R_0 is approximated by an Gaussian, and the mean-square fluctuation σ^2 is defined by:

$$\sigma^2 = < R^2 > - R_0^2. \quad (2.5)$$

In this approximation, the largest number of low energy particles can be found at R_0. The relative Gaussian distribution function:

$$f_1 = exp[-(R-R_0)^2/2\sigma^2] \quad (2.6)$$

is plotted in Fig. 2.3(b). It has a FWHM of 2.35 σ and $f_1 = 61\%$ when $|R-R_0| = \sigma$. The range straggling parameter σ/R for protons of kinetic energy E in some elements can be found in Ref.[37]. For example, σ/R is 1.38% for Be and 1.56 % for Al at beam energy of 5.9 MeV. At 21 MeV (where we did initial demonstration experiments) the numbers are 1.25% (Be) and 1.37% (Al).

When a heavy particle collides elastically with a target nucleus, the Coulomb force from the nucleus deflects it by Rutherford scattering. The angular distribution of the transmitted particles passing through a thin foil is mainly determined by nuclear multiple scattering. A cumulative effect of many nuclear scatterings will make a significant deviation from the original direction of a particle. The collisions with electrons produce only a small angular scattering of heavy particles. The importance of multiple scattering from nuclei for particle trapping is discussed in Section 3.5.

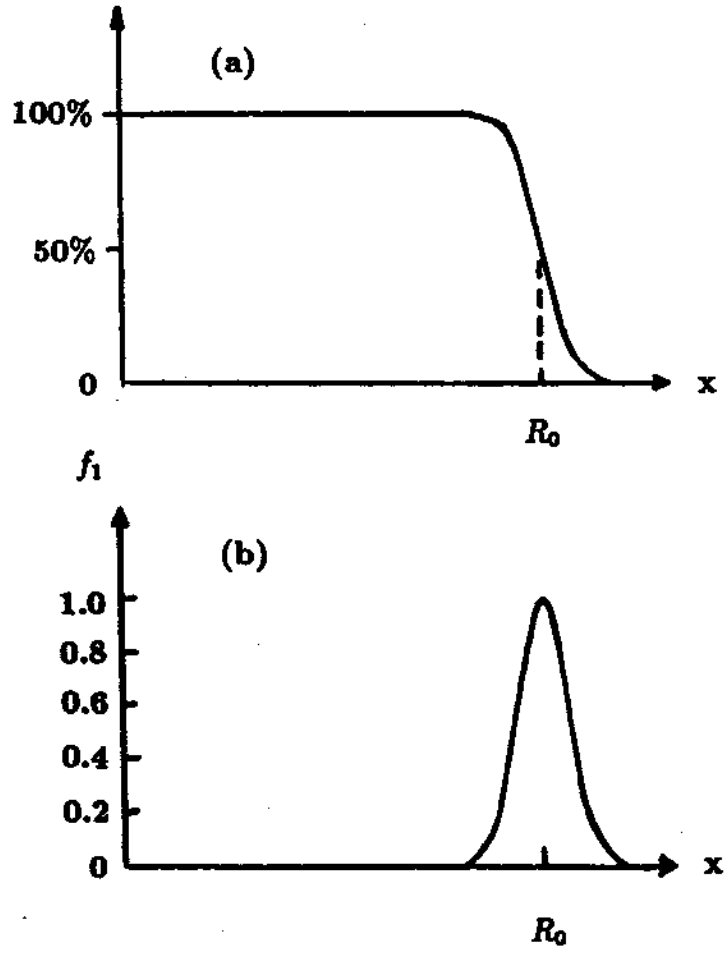

Figure 2.3: (a) An idealized range curve showing the fraction of particles in a beam penetrating to a given depth x. The mean range R_0 is the point passed by half the particles. (b) The relative distribution of particles near mean range.

2.3 Experimental setup for slowing protons and antiprotons in matter

The main purpose of the experiment is to obtain as many low energy antiprotons as possible. It is necessary to adjust the degrader thickness to just "range out" particles at the beam energy. Slow extraction is the normal mode of operation at LEAR in which a slow and uniform spill of up to 10^9 particles is sent to experiments over approximately 1 h with rates available from 10^3 to 10^5 Hz. Experimental methods of range measurements are discussed in Ref. [39]. A simple way to perform the experiment is by the transmission method. The basic idea of the transmission method for range curve and energy distribution measurements is illustrated in Fig. 2.4. A particle in the incident beam first goes through a Start detector, the parallel plate avalanche counter (PPAC), which provides a start signal and itself is also a part of the degrader. The particle then moves into a stack of thin foils and gases. If the particle passes through all the degrading material it can be counted by the microchannel plate detector (MCP) [40] which we used at both 300 and 77 K, to provide a stop signal from the transmitted particle. The time-of-flight Δt of the particle in passing from the degrader to the back detector over a distance L is recorded. If the degrader material is unchanged, a time-of-flight distribution can be obtained when a large number of particles are detected. From the flight time $\Delta t = L\sqrt{m_p/2E}$, we obtain the energy distribution of the transmitted particles and the low energy particle yield. The range curve can be traced out by changing the thickness of degrader and plotting the transmitted ion fraction, given by the ratio S_{stop}/S_{start} of the Stop detector counting rate and the Start detector counting rate, versus the thickness of the degrader.

A simplified logic diagram for the detection electronics is given in Fig. 2.4. It shows that signals from detectors are amplified, and then shaped by constant fraction discriminators before being sent to counters. Scalers count the signals from

both detectors. A qVt multichannel analyzer (LeCroy 3001) operating in the time analysis mode records the time delay between start and stop signals, as does a time-amplitude-convertor (TAC) plus an analog-digital-convertor (ADC). A microcomputer collects and stores the data, and displays the time spectrum.

The Stop detector subtends a finite solid angle to the center of the last surface. The half-angle in the side view plane θ_0 is 21^0 in this experiment, because the distance L is 2.54 cm and the MCP detector has an active diameter of 2 cm. Transmitted particles deflected away from beam axis by multiple scattering with $\theta < \theta_0$ will be counted.

2.3.1 The variable degrader for energy tuning

For incident 21 MeV antiprotons, we rotated thin degraders in and out of the beam [8]. This was not possible for 5.9 MeV antiprotons because the degraders must be 10 times thinner (0.25 mm Al). These degraders must also be located within the bore bore of the superconducting solenoid (See Fig. 3.3) to avoid large loss from multiple scattering. We use **dE/dx gas cells** to fine tune the degrader thickness for a given beam energy thus yield maximum number of low energy antiprotons for trapping. The apparatus used for proton and antiproton tests at about 6 MeV is as follows. High energy particles extracted from the machine through a thin titanium window enter from below at a rate of 1 to 10 kHz. To vary the energy loss of the particles by a small amount, we use two gas cells indicated in Fig. 2.5. Either SF_6 or N_2 at a pressure of 1 atm is kept flowing slowly through gas cell 1. The energy loss in the N_2 is smaller than the energy loss in the SF_6 by approximately 250 keV so the energy of the protons and antiprotons leaving gas cell 1 can be changed discontinuously by this amount. A mixture of SF_6 and He, also at 1 atm, is sent through gas cell 2. The mix can be adjusted continuously

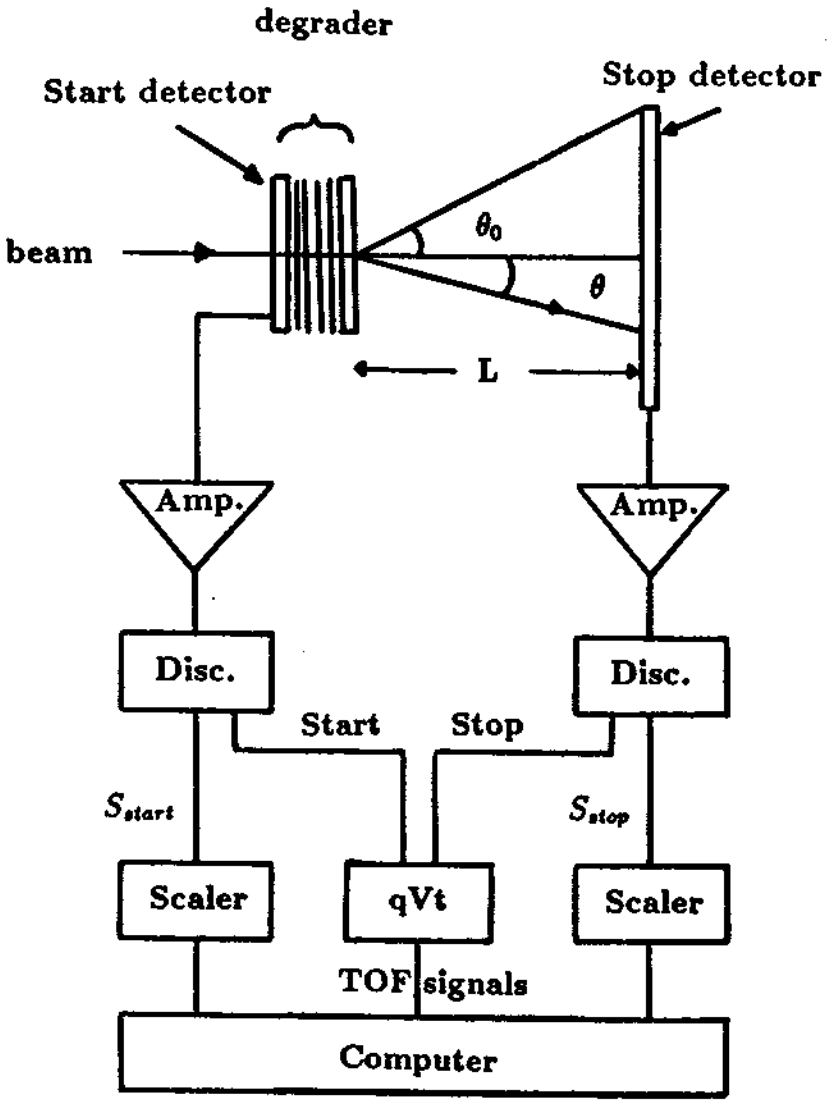

Figure 2.4: Transmission method for range curve and energy distribution measurements.

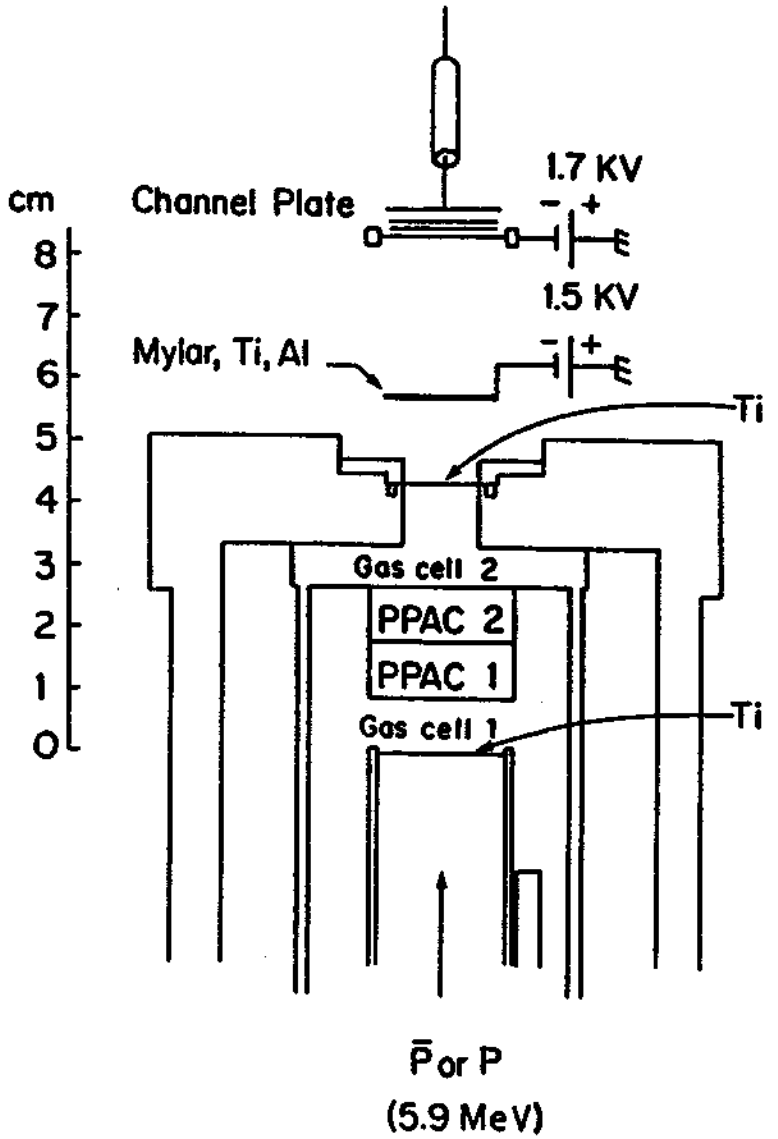

Figure 2.5: Time-of-flight apparatus. The apparatus from below 5 cm on the vertical scale remained in place for trapping experiments so that the incident antiprotons could be monitored and their energy tuned slightly. PPAC is the parallel plate avalanche counter.

with electronically controlled flow meters, allowing the energy of the antiprotons leaving gas cell 2 to be continuously adjustable over an additional 500 keV when the number of molecules in the mixture is changed from 0% SF_6 (i.e., 100% He) to 100% SF_6 (i.e., 0% He). These energy shifts were calibrated using the variable energy proton beam of the tandem accelerator of the Nuclear Physics Laboratory at the University of Washington, in Seattle, to produce range curves such as those in Fig. 2.9 which are discussed later. The energy loss was linear in the percentage of SF_6.

Helium and SF_6 flow in gas cell 2 are controlled by an OMEGA electronics package (FMA-2DV) with dual channel and setpoint potentiometers, and two OMEGA electronic mass flow controllers (FMA-116). The mass flow can be read and set for flow measurement and control by the package FMA-2DV unit. It can power and operate 2 independent flow controllers simultaneously. The display for reading flow value is linear with a $0-100\%$ full scale. The display shows the flow value when in the READ mode and the set point when in the SET mode. The mass flow controllers FMA-116 directly monitor the flow of gas molecules. This flow meter uses a heated sensing element and thermodynamic heat conduction principles to determine the true mass flow rate with 1% accuracy and 0.2% repeatability. The response time is 1 second. The mass flow controllers are factory calibrated for nitrogen (N_2). Nitrogen flow range is from 0 to 1 litre/min. The actual flow rate for any gas is equal to the flow rate of nitrogen unit times the correction factor. The correction factors for various gases are available from OMEGA Engineering Department. It is 1.45 for helium and 0.27 for SF_6. That is, when the flow display is 100%, the actual flows for He and SF_6 are 1.45 l/min and 0.27 l/min, respectively. In our system we use $SF_6\%$ as the percentage of molecules (or reference fraction) in the gas cell 2. The total flow is kept at 0.27 l/min. The corresponding helium setting (to keep the total flow constant) can be calculated as:

$$He(READ/SET) = 18.6 \times (100\% - SF_6\%). \tag{2.7}$$

For example, we need to set SF_6 at 10 and He at 16.7 to have 10% SF_6 and 90% He in gas cell 2. If we need 90% SF_6 and 10% He, then the setting should be 90 for SF_6 and 1.86 for He.

A simple **time-of-flight apparatus** (see Fig. 2.5) is used for proton and antiproton tests. A beam of 5.9 MeV particles extracted from LEAR through a thin (10 μm) titanium window, enter this apparatus from below at a rate of 1 to 10 kHz. Gas cells 1 and 2 permit particle energy tuning. Two PPACs located between the two gas cells determine when a proton or antiproton enters the apparatus with near unit efficiency and nanosecond resolution. Typically, the beam is focused into a spot diameter of less than 6 mm (full width half maximum) on the PPACs. The antiprotons slow in several layers of material needed for the trapping experiments being prepared. Each layer is listed in order in Table 2.1, along with the equivalent thickness of aluminum (to allow easy comparisons) and the approximate energy loss [41] in each layer. As shown in Table 2.1, most of the slowing, nearly 4 MeV, occurs in the final aluminum layer. The aluminum foil has mirror surfaces with very little surface roughness. The antiprotons stop and are detected with near unit efficiency in the channel plate detector located 2.5 cm down beam. The final degrader window and the channel plate are biased as indicated to minimize the probability of detecting a secondary electron liberated from the aluminum. The number of coincidences of the PPAC detectors with the channel plate are divided by the number of PPAC counts to give a measure of the fraction of the incident particles transmitted through the degrader. This gives the range curve when the number versus the equivalent thickness of the aluminum degrader is plotted. It will be discussed in connection with the Barkas effect below. Time-of-flight spectra of the transmitted protons and antiprotons are also recorded, making it possible to study the energy spectra of the transmitted protons and antiprotons.

Material	Equivalent thickness of Al (μm)		Energy loss (MeV)	
10-μm-thick Ti	16		0.21	
Gas cell 1 with N_2	4.4		0.06	
with SF_6		23		0.31
PPAC 1	11		0.16	
PPAC 2	11		0.16	
Gas cell 2 with He	1.4		0.02	
with SF_6		34		0.52
10-μm-thick Ti	16		0.24	
51-μm-thick Mylar	31		0.52	
10-μm-thick Ti	16		0.27	
117-μm-thick Al	117		3.70	
Total	224	275	5.34	6.09

Table 2.1: Matter traversed by protons and antiprotons.

2.3.2 The detection system

A chevron-pair **microchannel plate detector** with an active diameter of 20 mm (Varian 8960ZS) is used as the stop detector. It is used at 300 K (and with higher gain at 77 K). The gain for each plate is approximately 10^4 at about 850V bias potential. For the MCP pair at bias potential of 1700V, the total maximum gain is 10^8. The efficiency of the MCP is about 65% for fast particles measured by the transmission method (the coincidence signals of PPAC and CP divided by PPAC signals). The detection efficiency should be around 60 to 85% (see Ref. [40]) for low energy particles (2 to 50 keV). We use one as the detection efficiency for conservative number counting which allows a lower limit of the particle yield. Signals detected by MCP are denoted CP.

A beam diagnostic system of two **parallel plate avalanche counters** (PPAC) with position sensitivity was developed [42] as the Start detector for diagnostics of the incoming beam intensity and position (focusing). It meets the requirements for thickness (only 10% of the total Al degrader equivalent), time resolution (<0.5 ns), beam profile resolution (2.5 mm in both X and Y directions), and works well in the environment of the 6 T magnetic field.

PPACs are usually used in heavy ion detection for precise timing measurements in nuclear physics [43]. This type of gas counter with large active area is more useful when combined with position sensitive counters to have both timing and position information. The problem with light ion detection is that the specific ionization is much smaller as is the signal. However at an energy of a few MeV, ionization in the gas is high enough even for light particles due to the velocity dependency of dE/dx that a detection efficiency of nearly unity is achievable.

Each PPAC consists of two parallel aluminized mylar foils as electrodes, sepa-

rated by a narrow gap L to achieve good time resolution. The gap is normally filled with isobutane gas (C_4H_{10}). An energetic particle moves through the counter perpendicular to the foils, and electron-ion pairs are produced in the gas. When the high voltage V applied across the electrodes is sufficiently large, the homogeneous strong electric field V/L makes secondary ionization and an avalanche is formed. The number of secondary electrons produced by one primary electron is given by $e^{\alpha l}$, where l is the distance from primary electron initial location to the anode, the drift length. The α is the first Towsend coefficient, the mean ionization probability per unit path length and is a function of the reduced field strength V/Lp, here p is the gas pressure:

$$\alpha/p = A\ exp[-B/(V/Lp)]. \tag{2.8}$$

A and B are constants for the specific gas. In our system, the reduced field strength is 120 V/cm/torr for V = 900 Volts, L = 1.25 mm, and p = 60 Torr. Primary electrons produced near the cathode have the longest drift length L and hence the largest gain $e^{\alpha L}$. They contribute most to the signal. We denote the total number of primary electrons as N_0, and assume they are produced uniformly from l = 0 to L. Then the total number of secondary electrons within the gap generated by a single energetic proton or antiproton is:

$$G = \int_0^L (N_0/L)e^{\alpha l}dl = N_0(e^{\alpha L} - 1)/\alpha L. \tag{2.9}$$

Since $e^{\alpha L} >> 1$, the effective gain of the PPAC is:

$$G = N_0 e^{\alpha L}/\alpha L. \tag{2.10}$$

In our case, a 5.9 MeV proton or antiproton makes about 100 primary electrons, the effective gain G is about 10^6 for αL = 12. The resulting signal has an amplitude of about a 5 mV on a 50 Ω impedance with a 2 ns width and a very fast rise time due to the motion of electrons. Positive ions are collected over about 1μs and are too weak to see. With further amplification ($\times$ 100), a 500 mV signal can be observed by a 350 MHz scope and is fed into a discriminator for processing.

In each PPAC, the anode mylar is stretched and epoxied to a PC board disk. The cathode is stretched over a lucite boss contour to minimize breakdown at the edge of the active region and epoxied to another PC board disk. The active area has a diameter of 1.8 cm. Two PPACs with their gas lines and RG174/U coaxial cables are mounted in a 5 cm diameter by 3.5 cm long lucite assembly. Two 9 μm thick mylar vacuum windows supported by 125 μm thick 90% transparent molybdenum grids seal the detector assembly at both ends from the 1 atm ambient. The isobutane gas flow rate can be controlled up to 100 atm-cc/min. In Fig. 2.6(a), the two anodes are each etched into five parallel segments. Each of the 3 at the center is 2.5 mm wide. The position resolution of 2.5 mm is achieved in both X and Y directions when the first PPAC segments (X) are perpendicular to the second (Y). The PPAC detectors and their electronics are shown in Fig. 2.6(b). The ten segments (5X, 5Y) are brought to two stages of Phillips 776 amplifiers (each has a gain of 10) and discriminators. For continuous beam flux ($10^3 - 10^4$ particles/sec) the discriminator signals are sent to a 10-channel rate meter with 0.1 sec integration time constant. The 0 to 10 V analog output for each channel is fed into an LED display for X and Y beam profile histograms.

The electronics and logic circuits are shown in Fig. 2.4 and Fig. 2.6. Similar to the PPAC signal, the microchannel plate signal CP is amplified by a factor of 100 and shaped by a discriminator. The NIM pulses of the PPAC (x1, x2, x3, x4, x5, and y1, y2, y3, y4, y5) and CP are sent to scalers, and a logic unit (AND/OR logic). The important logic signals obtained are the start signal,

$$S_{start} = PPACX \bigcap PPACY, \tag{2.11}$$

and the stop signal,

$$S_{stop} = CP \bigcap PPACX \bigcap PPACY = CP \bigcap S_{start}, \tag{2.12}$$

where PPACX = $x2 \bigcap x3 \bigcap x4$, and PPACY = $y2 \bigcap y3 \bigcap y4$. As discussed earlier, S_{stop}/S_{start} determines the range curve, and relative timing of S_{stop}, S_{start} gives the

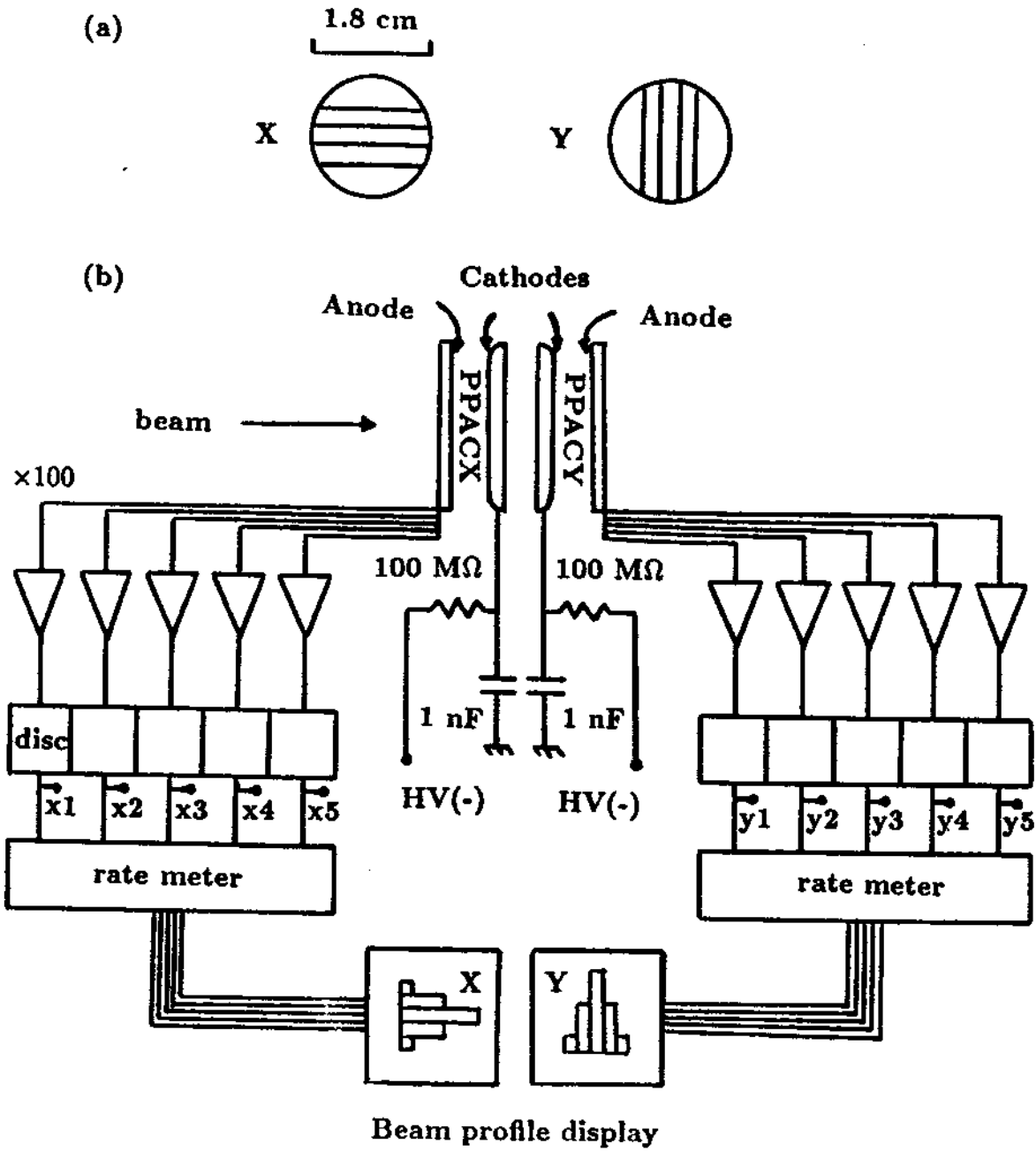

Figure 2.6: (a) The anodes of PPACX and PPACY. (b) PPAC detectors and their electronics.

energy distribution information.

2.4 Low energy antiproton yield and energy distribution of transmitted particles

A preliminary degrader test was carried out for 21.3 MeV antiprotons passing through Be [8]. The number of antiprotons which emerge from the degrader with low kinetic energy (along the beam axis), between 2 and 8 keV, is peaked at about the half intensity point in the range curve for antiprotons of all energies. Approximately 1 in 10^4 of the incident antiprotons emerges from the degrader with energy below 3 keV. The reason for using a 5.9 MeV beam instead of 21 MeV antiprotons is that a higher yield of low energy antiprotons is expected. The straggling parameter σ/R is essentially unchanged, but the range drops by nearly an order of magnitude when the energy is reduced from 21 MeV to 6 MeV. The distribution width (FWHM) ΔR therefore is reduced by an order of magnitude. Particles will stop in a much narrower slice of degrader. For example, the range in Be for 21 MeV beam is 3.0 mm with $\Delta R = 0.088$ mm while the range in Al for the 5.9 MeV beam is 0.25 mm with $\Delta R = 0.0093$ mm. The distribution is narrower by a factor of 9.5. Under ideal circumstances, we might thus expect 9.5 times more low energy antiprotons.

Fig. 2.7 shows the energy distribution of 5.9 MeV antiprotons after they pass through a degrader adjusted to give maximum low energy antiproton yield when the percentage of SF_6 in the gas cell is 60%. There are 5.1×10^5 Start signals and 10^5 Stop signals counted by scalers for this run. The normalized transmitted fraction is about 40%. The channel numbers (thus the flight time), kinetic energies, and the counts are indicated. Each channel represents 0.1 ns. The small bumps

before the TOF peak may be due to the antiproton annihilation secondary or the PPAC ringing that triggered the start counter. Because the gates of our discriminators were set at 60 ns, the signals from ringing reflect the TOF events after the 60 ns flight time. However, they do not affect the information we need, which is the spectrum within 60 ns and after the main TOF peak. The solid line is for a constant energy distribution of 100 counts/keV. The line fits the data well at the energy below 500 keV indicating that the particle energy distribution is fairly flat, and it falls when energy is near and above 500 keV. The average antiproton yield below 500 keV is approximately 2×10^{-4}/keV. Antiprotons between 20 ns and 40 ns correspond to the kinetic energies of 8 keV down to 2 keV. Changing the percentage of the SF_6 gas in gas cell 2 gives the antiproton yield between 2 to 8 keV versus the effective degrader thickness, as is plotted in Fig. 2.8. The peak yield is $1.6(0.1) \times 10^{-4}$/keV (which is a lower limit since we used 1 as the detection efficiency) when SF_6 in gas cell 2 is 60%, which is very close to the degrader setting of the half intensity point for antiprotons of all energies (see Fig. 2.9). It is approximately a factor of 8 increase compared with the previous test of 21.3 MeV beam traversing Be target ($2.1(0.1) \times 10^{-5}/keV$, also a lower limit). The surface roughness could make things worse. Only 1.7 μm broadening is needed to decrease the yield by 17%. There are about 20 surfaces in the degrader foils. If each surface contributes 0.4 μm in average (which is possible in our experiment), then it could make such difference. We observed this effect as many fewer antiprotons were trapped when very rough degrader surfaces were used.

Even though the proton data we have is only 10% of antiproton data, we can still qualitatively say that the energy distribution of protons emerging from the degrader is similar to the one for antiprotons. The low energy proton yield is $2.0(0.2) \times 10^{-4}$/keV which is consistent with the antiproton yield.

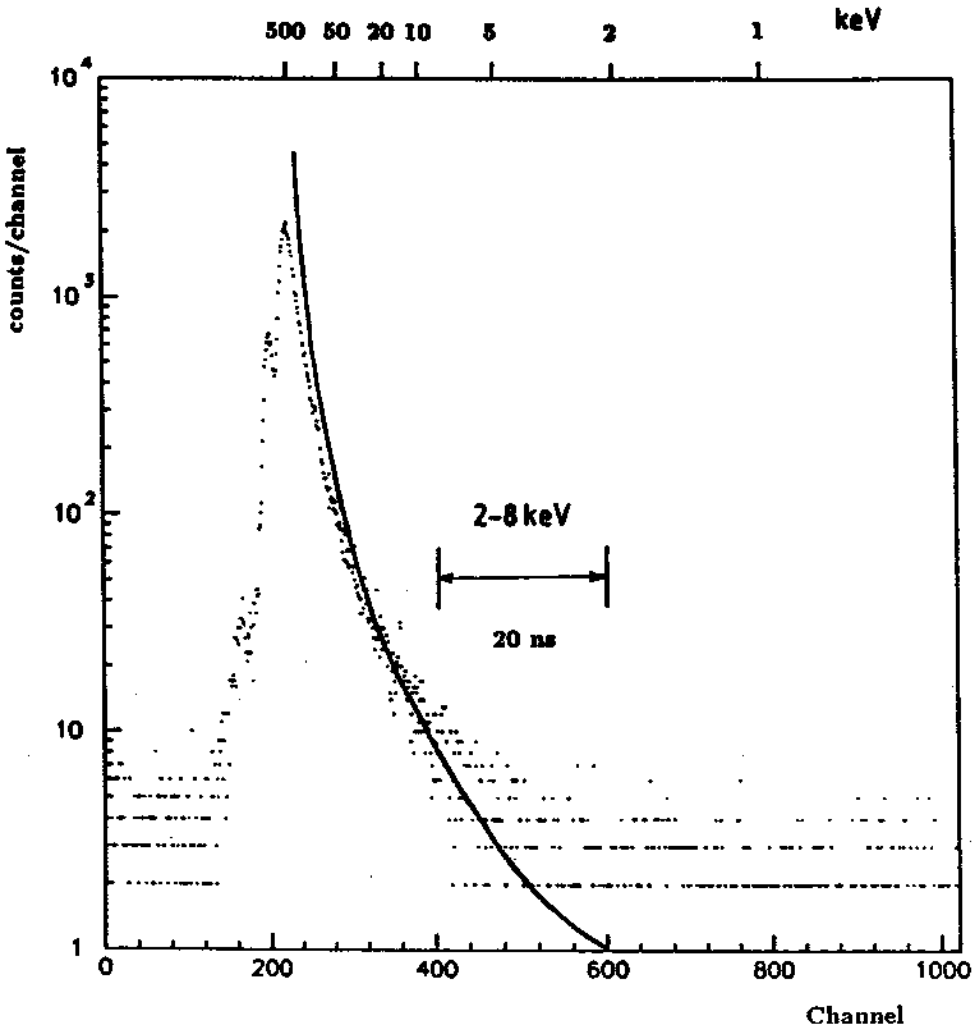

Figure 2.7: Energy distribution of exit antiprotons through degrader with maximum low energy particle yield.

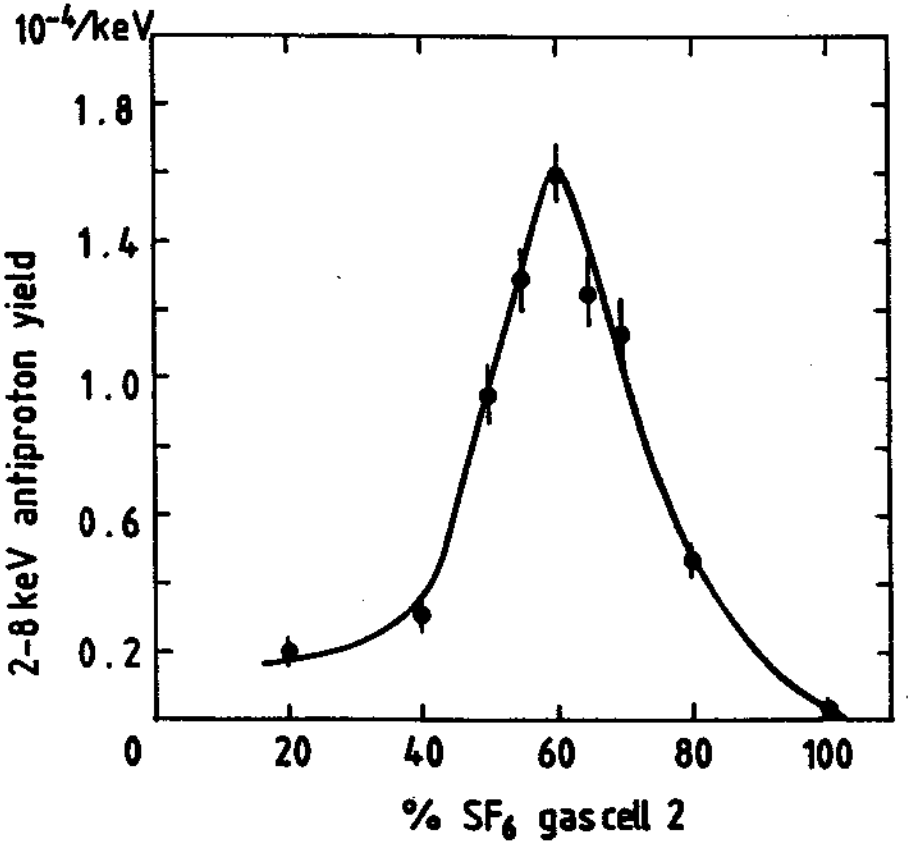

Figure 2.8: 2 to 8 keV antiproton yield versus the effective degrader thickness for 5.9 MeV antiprotons in the apparatus shown in Figs. 2.4 and 2.5.

2.5 Observation of the Barkas effect with protons and antiprotons

Energy-loss and range measurements carried out to improve our understanding of charged heavy particle penetration of matter appear to be of great interest for basic and applied physics. Barkas and his collaborators [44] first observed the striking difference of the energy loss processes in emulsion track studies for π^+ and π^-, and also for Σ^+ and Σ^-. The difference in the range of heavy particles of opposite charge under otherwise identical conditions is known as the Barkas effect. This charge-sign-dependent effect comes from distortions of the target electron motion or wave function during the atomic collision, so it is also referred as the polarization effect. For a heavy particle of charge Z and velocity v passing through a medium of atomic number Z_t, the stopping power S may be written as

$$S = -dE/dx = (4\pi e^4/mv^2)NZ_tZ^2(L_0 + L_1Z + L_2Z^2) \qquad (2.13)$$

where N is the atom number density of the stopping element, m is the electron rest mass, and L_0, L_1 L_2 are functions of the particle velocity and stopping material. Here, higher-order terms in Z are included unlike the Equation (2.3). The existence of a Z^3 term with a positive coefficient L_1 implies a greater range for a negative particle than for a positive one under conditions of equal mass and equal initial velocity. With protons and antiprotons of the same energy, observed differences in the stopping power and range arise only from L_1 (higher-order terms odd in Z are neglected here). The effect of the terms of even order in Z cancel.

Observations of the Barkas effect using positive and negative muons have been reported [45,46]. Higher order terms in the stopping power have been accurately measured for positive ions of H, He and Li [47]. There are many other ion experiments and the available experimental data indicates a positive coefficient L_1. Theoretical investigation of Z^3 correction was made first by Ashly, Ritchie and

Brandt [48](ARB theory) and later Jackson and McCarthy [49] and by Lindhard [50] in classical calculations. Though in general they agree well with experiments qualitatively, current analytical results differ by approximately a factor of 2, and there are even larger discrepancies arising from numerical calculations.

The range curve data obtained verified the existence of the Barkas effect for the proton-antiproton system [10]. The points in Fig. 2.9 represent two measurements of the number of transmitted projectiles versus the effective thickness of the degrader. The left curve is for protons, the right curve is for antiprotons. The vertical scale is proportional to the coincidence signal divided by the number of incident projectiles, as described earlier. A small and flat pion background of $\approx$ 10% (from annihilation pions striking the channel plate) was subtracted off in the case of the antiprotons. The horizontal scale indicates the fraction of SF_6 in gas cell 2 with either N_2 in the first gas cell (tick marks above the axis) or with SF_6 in the first gas cell (tick marks below the axis). The horizontal scale thus essentially represents the thickness of the degrader. Increasing the aluminum thickness by 51 μm would cover the same range covered by this scale. Alternatively, the horizontal scale represents the relative scale corresponding to a shift of approximately 750 keV in the incident energy. The shift of the proton range curve as a function of incident proton energy was used to calibrate the gas cells.

The error bars on the measured points in Fig. 2.9 represent the largest variations observed in the measured points over several hours. These variations were observed to be correlated with beam intensity, beam steering, etc. The size of the points themselves represent the short-term repeatability over several minutes. The proton and antiproton curves have a similar shape, as illustrated by the identical smooth curves sketched through the measured points, but the antiproton curve is shifted by 150$\pm$20 keV. Several corrections and additional uncertainties must be included. The LEAR staff measured the difference in beam energy between

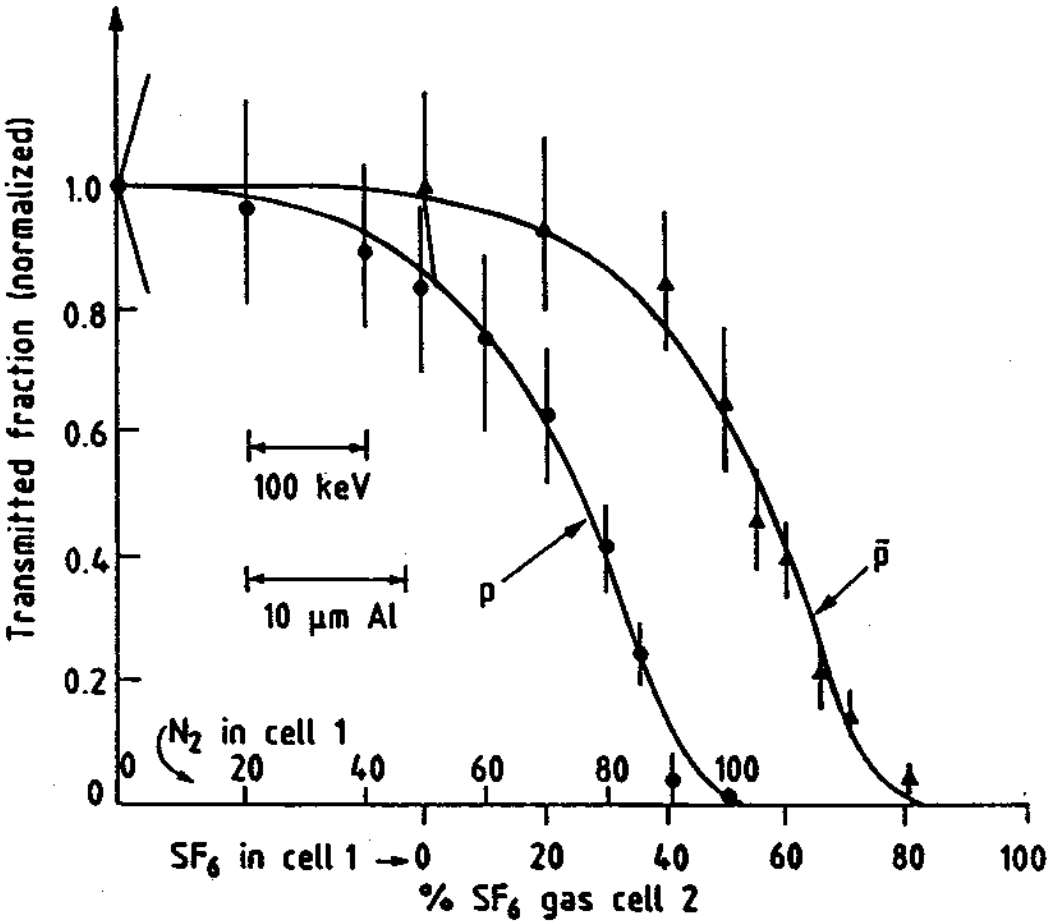

Figure 2.9: Normalized fraction of antiprotons detected after the degrader showing the difference in energy loss and range of protons (left) compared to antiprotons (right).

protons and antiprotons extracted from LEAR to be 13±12 keV. Temperature differences in the degraders between the proton and antiproton measurements contribute 31±12 keV. Uncertainties in the calibrations of the first and second gas cell contribute ±30 keV and ±20 keV, respectively. The net result is that the energy lost by 5.9 MeV protons is greater by

$$\Delta E = 194 \pm 45 \; keV \tag{2.14}$$

than the energy lost by 5.9 MeV antiprotons. The aluminum equivalent for this energy difference is $\Delta R = 14\mu$m and

$$\Delta R/R = 5.6 \pm 1.4\% \tag{2.15}$$

is the equivalent fractional range difference in aluminum, the range being larger for antiprotons.

To quote the above range difference for aluminum and to compare with theoretical values, we initially model the degrader as a piece of aluminum approximately 250-μm thick. This is the sum of the equivalent Al thicknesses from Table I. The formula given by the theory of Ashley, Ritchie, and Brandt (ABR) [48] gives a fractional range difference of 3.2%, which is somewhat lower than our measured value. However, Lindhard included the contributions from close collisions which are absent in ARB theory and estimated that the Barkas effect was approximately twice that of ARB theory [50]. To accommodate this effect, Ritchie and Brandt [51] adjusted their original choice of cutoff at small impact parameters to make the L_1 larger. Both the Lindhard theory and the adjusted ARB theory seem to agree with our measurement, though more precise theoretical predictions are clearly needed. To check the simplifying model above, we use the Lindhard theory to estimate that modeling the matter traversed by the beam as a single piece of aluminum could cause an error as large as ±20 keV, somewhat smaller than the uncertainty from other sources. Thus we can consider ΔE given earlier to be the measured

energy loss in Al, provided the quoted uncertainty is increased to ±50 keV. The reason that the Barkas effect occurs primarily in the aluminum is that until they enter the final aluminum degrader at approximately 4 MeV, both the antiprotons and the protons travel rapidly enough so that contributions to the Barkas effect are small.

In summary, the Barkas effect of about 6% difference in range is detected when 5.9 MeV protons and antiprotons are sent through the same aluminum degrader [10]. Another measurement of the Z^3 contribution to the stopping power using protons and antiprotons in silicon is reported in Ref. [52].